This article has been accepted for publication in IEEE Transactions on Wireless Communications. This is the author's version which has not been fully edited and content may change prior to final publication. Citation information: DOI 10.1109/TWC.2023.3284897

Efficient Exclusion Strategy of Shadowed RIS in Dynamic Indoor Programmable Wireless Environments

Zi-Yang Wu, *Member, IEEE*, Muhammad Ismail, *Senior Member, IEEE*, and Jiao Wang

Abstract

Recent efforts have promoted programmable wireless environments (PWEs) to enhance the reception quality in high-frequency bands via reconfigurable intelligent surfaces (RISs). However, relevant research efforts are limited to setups with stationary users. This paper shows that crowd mobility in indoor PWEs induces spatio-temporal shadows on the surfaces, resulting in spatio-temporal sparsity in channel gains due to signal blockages. This overlooked aspect impacts the operation strategy of PWEs as the shadowed RIS tiles would contribute to the overheads while offering almost no improvement to the reception quality. Hence, this paper proposes an optimal strategy that excludes the shadowed tiles, which maximizes the utilization efficiency of RISs while minimizing the overheads. Since signal blockage is tied with the details of user mobility, a general model does not exist to identify such shadowed tiles for exclusion. Hence, we follow a data-driven approach that capitalizes on a realistic indoor mobility model and ray-tracing to generate the channel data. However, conventional ray-tracing presents high complexity that hinders data generation. So, we propose an approach to identify the shadow regions with a nine-order of magnitude reduction in complexity to efficiently generate the channel data. Furthermore, we present two exclusion strategies that offer guaranteed and best-effort quality-of-service support, and each can identify the tiles to be excluded via a search method with a complexity of $\mathcal{O}(N)$ for N tiles. The results indicate that the proposed strategies reduce the overheads by $45-50\%$ while maintaining optimal service quality in various environments, operation frequencies, and user and access point density.

Index Terms

Millimeter wave (mmWave), visible light communications (VLC), intelligent reflective surfaces (IRS), reconfigurable intelligent surfaces (RIS), mobility, resource allocation.

Z.-Y. Wu and J. Wang are with the College of Information Science and Engineering, Northeastern University, Shenyang 110819, China (email: {wuziyang, wangjiao}@ise.neu.edu.cn). M. Ismail is with the Department of Computer Science, Tennessee Tech University, Cookeville, TN 38505 USA (email: mismail@tntech.edu). This paper was presented in part at the IEEE International Conference on Communications (ICC), Montreal, QC, Canada, June 2021 [1]. The work of Dr. M. Ismail is supported by NSF ERI Award 2138234. Dr. Wu are in part supported by the NSFC under Grant 62103088, the Fundamental Research Funds for the Central Universities under Grant N2104024, and China Postdoctoral Science Foundation Award 2021M700723.

I. Introduction

The wireless channel has always been regarded as an uncontrollable entity that negatively impacts the received signal quality. Hence, pre- and post-processing of wireless signals have been carried out at the transmitters and receivers to compensate for such negative impacts. However, the fundamental limits imposed by the wireless channel will eventually represent a bottleneck in the face of growing traffic demands and their stringent quality-of-service (QoS) requirements [2]. To address this challenge, it has been envisioned that the wireless channel in the next-generation networks will be transformed into a programmable entity that can be jointly optimized with the transmitter and receiver to achieve the target QoS [3]. Enabling a programmable wireless environment (PWE) is possible through the adoption of reconfigurable intelligent surfaces (RISs) in a near-passive manner [4]–[6]. An RIS is an inexpensive thin material that covers parts of the walls to optimally reshape/reflect the incident waves in a way that improves the received signal quality using a minimal power consumption (i.e., in a nearly-passive manner). These RISs are realized using a large number of inexpensive small antennas or smart meta-surfaces [7].

Recent research efforts have demonstrated that the RIS overheads represent a limiting factor to the expected gains from PWEs [8], [9]. The overheads include signaling and power consumption associated with channel estimation, user-tile assignment, and optimal configuration of the tile reflection parameters. Such overheads are proportional to the number of RIS tiles [9]. In a dynamic environment with user mobility, re-assignment of users to RIS tiles and reconfiguration of the tile parameters will take place frequently. Hence, further efforts are required to ensure that minimal overheads are introduced in order to maximize the attained gains in PWEs. This paper proposes efficient strategies to reduce such overheads in dynamic indoor PWEs through the exclusion of ineffective RIS tiles that do not contribute to significant improvement in QoS.

A. Related Works

PWEs can play a vital role in next-generation wireless networks that rely on high-frequency bands for communications, such as the millimeter wave (mmWave) [10] and visible light (VL) bands [11]. This is mainly because of the limited diffraction capabilities of line-of-sight (LoS) signals at such bands and their susceptibility to blockage, especially in mobile environments [12]. In this context, RIS can reflect the non-LoS (NLoS) signals to support the target QoS whenever the LoS signal is absent [13]. Hence, recent research works have investigated the benefits of PWEs in the mmWave [10], [14], [15] and VL [16]–[18] bands.

Recent efforts have developed simple two-way channel models in PWEs [7]. However, these simple models do not account for user mobility. A better understanding is required regarding channel dynamics in realistic setups that consider user mobility. A framework is presented in [19] to model and simulate a PWE with multiple mobile users. Unfortunately, no details are given in recent works such as [19], [20] regarding the adopted user mobility model. The work in [21] presents RIS channel models within the mmWave frequency band. The presented models cover both indoor and outdoor scenarios while considering LoS outage probability and shadowing effects based on general statistical distributions. However, this contradicts our recent findings in [22], which demonstrate that the shadowing effects, channel gain statistics, and LoS outage probability do not follow a single/general distribution for indoor scenarios and rather depend on the spatio-temporal user mobility and its interaction with other users and the surrounding environment.

B. Motivations and Challenges

A thorough review of existing research in PWEs, as summarized in [23], demonstrates that pertinent efforts mainly focus on networking environments that consist of stationary user equipment (UE). Hence, existing research completely overlooks the impact of crowd user mobility on the channel gains in indoor PWEs. It is intuitive that in a dynamic environment not all of the deployed RIS tiles will be useful to communications due to users' mobility, which will introduce shadowed regions on the surfaces. The bodies of the users moving in the room along with the surfaces of other objects (e.g., furniture) will block the signals from the access points (APs) to reach specific regions on the walls and floor. A similar blockage is expected for the signals reflected from the RIS tiles towards the users. Consequently, the engagement of RIS tiles at the shadowed regions on the walls and floor are less likely to be beneficial in improving the QoS. The inclusion of such shadowed RIS tiles unnecessarily increase the operational complexity due to the associated overheads for channel estimation, optimal tile-user assignment, and the optimal configuration of the RIS tile reflection parameters.

Consequently, an efficient operation strategy should exclude the RIS tiles at the shadowed regions. However, it is quite challenging to identify such shadowed regions in an indoor layout. Our recent results in [22] have demonstrated that it is not practical to describe the channel gain and outage statistics of LoS and NLoS signals at high-frequency bands by a single/global model. Instead, such statistics highly depend on the room layout and the spatio-temporal mobility pattern

of the users. Hence, relying only on a model-based exclusion strategy will not lead to practical results. One alternative is to adopt a data-driven approach that identifies the shadowed regions in specific room layouts based on ray-tracing techniques. Unfortunately, adopting ray-tracing based methods with signal blockage judgment to identify such shadowed regions would incur heavy computational complexity given the large number of tiles across the room, as will be proved in Section III. Hence, conventional ray-tracing techniques would impede a data-driven-based exclusion strategy of ineffective RIS tiles.

C. Contributions

In order to address the aforementioned challenges and develop an efficient exclusion strategy of ineffective RIS tiles in indoor layouts, we have carried out the following contributions:

- We formulate and prove the convexity of optimization problems that exclude ineffective RIS tiles via balancing the attained QoS improvement for RIS-assisted communications with the utilization efficiency of RIS tiles in two cases, namely, guaranteed and best effort QoS support. Besides, we analytically derive optimal exclusion strategies for the aforementioned formulations that depend only on the statistics of the RIS channels.
- We propose a framework to generate indoor RIS channel data in dynamic indoor PWEs. The collected channel statistics are used to realize the optimal RIS tile exclusion strategies. The RIS channel generation framework relies on a multi-timescale UE-centric mobility model [22] that captures crowd mobility patterns in indoor scenarios while generating the channel data. Hence, the proposed framework unveils the impact of the interaction among mobile UEs and the surrounding environment on link availability with RIS tiles both in the uplink (UL) and downlink (DL).
- In order to efficiently realize the channel generation framework, we overcome the complexity of the blockage judgement in conventional ray-tracing methods by proposing the *Shadow Area Identification* method along with a numerical simplification of the *Equivalent Infinite Projection*. The shadow area identification method helps in addressing the complex ray-tracing blockage judgement problem via a simple look-up table that presents nine-order of magnitude reduction in computational complexity, hence, paving the way towards data-driven solutions in PWEs.
- Using the generated RIS channel statistics, we have validated our proposed RIS tile exclusion strategies in various indoor scenarios and over different transmission bands. The results

have proved the effectiveness of the proposed RIS tile exclusion strategies in terms of: (a) reduction in signaling overhead by $45-50\%$ and (b) improvement in RIS tile utilization efficiency by 15%. The proposed RIS tile exclusion strategies are found to be compatible with scenarios of: (a) varying user densities, (b) different AP densities, and (c) different transmission bands.

The proposed framework has been tested in three layouts that are commonly used in literature [5], [24]–[26]. However, when confronted with different layouts, the proposed framework is still applicable to exclude idle RIS tiles and reduce the controlling overhead. The applicability of the proposed method in this paper is not limited by spatio-temporal dimensions, as the RIS channel is subject to mobility constraints, which are characterized by scale-free statistics [27].

The rest of this paper is organized as follows. Section II presents the network model and Section III formulates the optimization problems and analytically derives the optimal policies related to RIS tile exclusion under QoS guarantee and best effort services. Section IV describes the proposed Shadow Area Identification method to efficiently generate the RIS channel statistics, and hence, realize the optimal RIS tile exclusion policies. The numerical experiment results and the associated discussion pertaining to the implementation of the RIS tile exclusion strategies are presented in Section V. Conclusions are made in Section VI.

II. Network Model

We first introduce an indoor environment covered with next-generation wireless networks. We consider three high-frequency bands, namely, 28 GHZ mmWave, 73 GHz mmWave, and VL bands. The mmWave and VL are at the far ends of the high-frequency bands, respectively, with considerably different diffraction capabilities. In VL bands, the difference of diffraction capabilities in 400 to 700 THz is negligible [26]. However, in mmWave bands, since the difference in different sub-bands is significant [28], we consider 28 GHz and 73 GHz to investigate the far ends of mmWave bands. Furthermore, we consider three types of room layouts.

A. Indoor Programmable Wireless Environment

Three types of indoor layouts are considered:

- R1: There is only one meeting desk at the room center as illustrated in Fig. 1. The desk size is 2m$\times$2m$\times$0.9m.

This article has been accepted for publication in IEEE Transactions on Wireless Communications. This is the author's version which has not been fully edited and content may change prior to final publication. Citation information: DOI 10.1109/TWC.2023.3284897

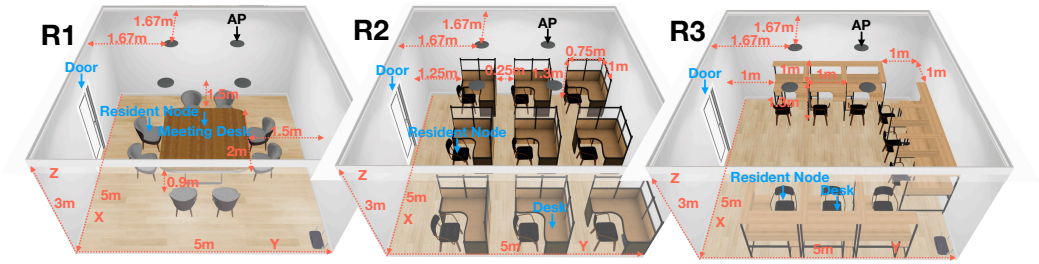

Fig. 1. Illustration of the room layouts. Mobile users, holding UEs that connects with APs via light or mmWave communications in DL and infrared (IR) or mmWave in UL, are assumed in these scenarios. The room layouts present $1,500$ RIS tiles on each wall to enable an indoor PWE.

- R2: There are nine desks with separators at height of 1.5m in total, which are evenly located in the room as illustrated in Fig. 1.
- R3: There are nine desks (with the same size as in R2) located along the sides of the wall, leaving the center of the room empty, as illustrated in Fig. 1.

For all layouts, the room size is $5\text{m} \times 5\text{m} \times 3\text{m}$, and there is only one entrance centrally located at (2.5m, 0m). There are four light APs or four mmWave APs distributed evenly on the ceiling plane. Examining these nine case studies (three room layouts and three transmission bands) help better understanding the unique features of PWEs under various wireless propagation conditions.

RIS tiles are deployed over the four walls of the room. To express the locations of the RIS tiles, each wall is described as a grid with each square representing a location of one RIS tile. For instance, at 28 GHz frequency, a meta-surface based RIS tile dimension is expected to be roughly $10\text{cm} \times 10\text{cm}$ square [19] such that the far-field condition holds for each tile. Hence, in the layout shown in Fig. 1, it is expected to have more than $1,500$ RIS tile locations per wall. The far-field condition is always fulfilled for VL as multi-input-multi-output methods can be applied for each reflector [29].

B. Indoor Practical Mobility Generation

One to eight users are assumed to enter the room successively and wander across the room following the indoor mobility model proposed in [22], such that the effect of crowd mobility is examined. At high-frequency bands and due to the sensitivity of the received signal intensity to the relative displacement between the transmitter and the receiver, the wireless channel depends not only on the UE trajectories and fading but also on the spatial relationship between the UEs and non-transparent objects. Our recent work [22] has proposed and validated a realistic indoor

This article has been accepted for publication in IEEE Transactions on Wireless Communications. This is the author's version which has not been fully edited and content may change prior to final publication. Citation information: DOI 10.1109/TWC.2023.3284897

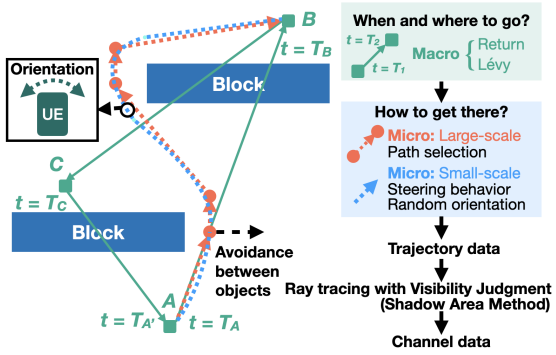

Fig. 2. An illustration on our proposed mobility generation procedures.

mobility model that captures the human mobility details on two timescales, namely, macro and micro scales. As demonstrated in Fig. 2, the macro scale specifies the time to move to the next destination point and determines that destination point based on a time-homogeneous semi-Markov renewal process that covers both return regularity and bounded Lévy-walk. On the other hand, the micro scale captures the mobility details while moving from one point to another by implementing the shortest path, steering behavior, and UE orientation. The steering behavior dominates the interaction among users and their surroundings and impacts the orientation of UEs. The synthetic user trajectory data generated by the mobility model of [22] has been validated against measurements using the Phyphox application.

To generate the dataset adhering to practical mobility, we determine the following parameters based on real-world measurements. The first key parameter is the displacement exponent which indicates the power-law distribution of destination selection. According to real-world measurements, this exponent was found to be approximately 0.5. As for the sojourn duration exponent featuring the power-law distribution of residential interval decision, we assume it to be 1 since this work only studies mobility impacts, and the detailed sojourn behavior is thus irrelevant. UE rotation is usually transferred into the spherical coordinate system with the polar angle and azimuth angle. The recent statistics [22] show that the polar angle subjects to Laplace distribution while sitting with a mean of 45.11 and a standard deviation of 7.84, and it follows Gaussian distribution when walking with a mean of 31.79 and a standard deviation of 7.61.

C. Indoor mmWave Channel Model

We consider two bands for the mmWave channels, namely, 28 GHz and 73 GHz. Each RIS tile is designed in a small size such that a far-field path-loss feature could be applied [7]. L_{LoS}

denotes the path-loss for LoS rays, and particularly, $L_{\mathrm{c,s}}$ accounts for the path-loss of the sub-rays in the NLoS clusters.

Define mmWave LoS channel gain from any transmitter (UE or AP) to RIS tile as [21]

$$\mathbf{G_m} = \mathbf{G}_{\mathrm{m,LoS}} + \mathbf{G}_{\mathrm{m,NLoS}}, \tag{1}$$

where

$$\mathbf{G}_{\mathrm{m,LoS}} = \sqrt{G_e\left(\theta_{\mathrm{LoS}}\right) L_{\mathrm{LoS}}} e^{j\varrho} \mathbf{a}\left(\phi_{\mathrm{LoS}}, \theta_{\mathrm{LoS}}\right), \tag{2}$$

$$\mathbf{G}_{\mathrm{m,NLoS}} = \gamma \sum_{c=1}^{C} \sum_{s=1}^{S_c} \beta_{c,s} \sqrt{G_e\left(\theta_{c,s}\right) L_{c,s}} \mathbf{a}\left(\phi_{c,s}, \theta_{c,s}\right), \tag{3}$$

$$L_{LoS/c,s} = -20\log_{10}\left(\frac{4\pi}{\lambda}\right) - 17.3\log_{10}\left(d_{LoS/c,s}\right) - X_\sigma \quad (\mathrm{dB}), \tag{4}$$

$$G_{\mathrm{e}}\left(\theta_{\mathrm{LoS/c,\,s}}\right) = 2(2q+1)\cos^{2q}\left(\theta_{\mathrm{LoS/c,\,s}}\right), \quad -\pi/2 < \theta_{\mathrm{LoS/c,\,s}} < \pi/2, \tag{5}$$

where it is assumed that the beams are grouped under C clusters and each cluster contains S_c sub-rays, and γ stands for a normalization gain factor among sub-rays defined by $\gamma = \sqrt{\frac{1}{\sum_{c=1}^{C} S_c}}$, $\beta_{c,s} \sim \mathcal{CN}(0,1)$ is the complex path gain, $\mathbf{a}(\cdot)$ is the RIS array response vector, ϕ and θ represents the azimuth and elevation arrival angles with respect to the RIS broadside, λ denotes the wavelength, d is the transmission distance, $X_\sigma \sim N(0, \sigma^2)$ is the fading term in logarithmic units, and $\varrho \sim \mathcal{U}[0, 2\pi]$. Consider the RIS tile's physical area as $(\lambda/2)^2$, which implies $q = 0.285$ [21]. For the reflected path from an RIS tile to the receiver (UE or AP), it is assumed that the NLoS component in the reflected link $\mathbf{G}_{\mathrm{m,NLoS}}^{\mathrm{RIS}\to\mathrm{UE/AP}}$ can be ignored compared to the LoS component $\mathbf{G}_{\mathrm{m,LOS}}^{\mathrm{RIS}\to\mathrm{UE/AP}}$ in an indoor environment [21]. However in the link from AP/UE to RIS, the NLoS component $\mathbf{G}_{\mathrm{m,NLoS}}^{\mathrm{UE/AP}\to\mathrm{RIS}}$ cannot be ignored as $\mathbf{G}_{\mathrm{m,NLoS}}^{\mathrm{UE/AP}\to\mathrm{RIS}}$ would be in the same order of magnitude of $\mathbf{G}_{\mathrm{m,LoS}}^{\mathrm{UE/AP}\to\mathrm{RIS}}$ [21]. Furthermore, once an LoS or sub-reflected ray is judged as blocked by any object (desks, another user, or the user's own body), the term $\mathbf{G}_{\mathrm{m,LoS}} = 0$, and the only reception belongs to $\mathbf{G}_{\mathrm{m,NLoS}}$. An efficient judgment approach of LoS blockage is proposed in Section IV.

D. Indoor Optical Channel Model

In the VL/IR band, the LoS impulse response among any two points is given by

$$G_{\mathrm{v}} = \begin{cases} \frac{A_{\mathrm{R}}}{d_{\mathrm{v}}^2} \frac{(m_{\mathrm{v}}+1)}{2\pi} \cos^{m_{\mathrm{v}}}(\phi) \cos(\psi) T_{\mathrm{S}}\left(\psi\right), & \text{for } 0 \le \psi \le \Psi_{\mathrm{c}}, \\ 0, & \text{for } \psi > \Psi_c \text{ or blocked}, \end{cases} \tag{6}$$

where A_{R} is the sensor area, d_{v} is the transmission distance, ϕ is the angle of irradiance, ψ is the receiver incidence angle, Ψ_{c} is the receiver's field-of-view (FOV), and T_{S} is the overall transmission response of the optical system. Besides, the mode number m_{v} is related to half power angle $\Phi_{1/2}$ via $m_{\mathrm{v}} = -\ln 2 \big/ \ln(\cos \Phi_{1/2})$. In this paper, it is assumed that the receivers' FOV is $90°$, A_{R} is 100 mm^2, and the AP transmitters are Lambert sources [22]. T_{S} is treated as 1 for simplicity as no lenses nor other optical devices are involved. Different from the mmWave channels, due to the lack of diffractions of light, once the LoS ray is blocked, only the reflected rays can be perceived. According to the real-world measurements in [30] and numerical analysis in [26] it is found that $\frac{G_{\mathrm{v,NLoS}}^{\mathrm{AP}\to\mathrm{RIS}} G_{\mathrm{v,NLoS}}^{\mathrm{RIS}\to\mathrm{UE}}}{G_{\mathrm{v,LoS}}^{\mathrm{AP}\to\mathrm{RIS}} G_{\mathrm{v,LoS}}^{\mathrm{RIS}\to\mathrm{UE}}}$ approximates to $0.0026 \sim 0.1437$. When the VL RIS tiles such as tunable liquid-crystals are configured as selective reflection and absorption, this ratio will be much lower since $N-1$ the number of effective reflective elements would be reduced to $0.3N-1$ [1]. Consequently, if the LoS ray is blocked, $G_{\mathrm{v}} \simeq 0$.

III. Problem Statement

The performance of RIS as a reflector in receiving UL and DL signals is identical in each separate band. Therefore, for simplicity, it is assumed that the antenna parameters of AP and UE are the same such that the DL (*AP*$\to$ *RIS* $\to$ *UE*) and UL (*UE*$\to$ *RIS* $\to$ *AP*) present very closed channel gain with respect to tile n as

$$G(n) = G^{\text{AP-RIS}}(n) \boldsymbol{\Theta} G^{\text{RIS-UE}}(n), \tag{7}$$

where $\boldsymbol{\Theta}$ describes the phase and reflection coefficient control matrix. To formulate an exclusion strategy, we have to value how much each RIS tile could contribute to the maximum extent and how much the mobility would impact each tile, instead of the overall functionality of the RIS. Since the size of each RIS tile satisfies the far-field condition, essentially, the beam of each RIS tile can be independently controlled, or in other words, the control matrix of each tile is independent. We assume that the control matrix of each tile can be well-designed so that the beam from each RIS panel tracks UE as a reflector, and hence the control matrix itself can be ignored. In what follows, we formulate the exclusion strategy of shadowed RIS tiles in two cases, namely, under QoS guarantee and best effort service.

A. Case 1: Guaranteed RIS Quality-of-Service and Efficient Utilization

Denote the set of RIS tiles across the room by $\mathcal{N}$. An RIS tile $n \in \mathcal{N}$ experiences an outage event either in the UL or DL with probability

$$P_{\mathrm{o}}(n) = \mathbb{E}_{t,u,a}\left[\mathbf{1}\left\{G(t,n|a,u) \leq G_{\mathrm{th}}\right\}\right], \tag{8}$$

where G_{th} represents an outage threshold on the received channel gain and $G(t,n|a,u)$ denotes the received channel gain at RIS tile n and time t while assisting the communications between UE u and AP a. The outage probability of tile n is described in (8) based on the expectation of outages over the time while considering the channels among all the UEs and APs. In what follows, the tile index n is ordered such that $P_{\mathrm{o}}(n)$ monotonically increases with respect to n.

In the guaranteed QoS support, the exclusion strategy of ineffective RIS tiles aims to guarantee an optimal average outage probability and utilization efficiency across the RIS tiles assisting the communications. This is done by not only excluding the long-term shadowed RIS tiles but also considering the RIS efficiency. This can be expressed as

$$\max_{\rho_n \in \{0,1\}} \eta(\rho_n) = \sum_{\mathcal{N}} \rho_n \left(\mathbb{E}_n\left[P_{\mathrm{o}}(n)\right] - P_{\mathrm{o}}(n)\right). \tag{9}$$

where ρ_n is a binary decision variable such that $\rho_n = 0$ means that RIS tile n is not involved in communication support (i.e., excluded), otherwise $\rho_n = 1$. In (9), $\mathbb{E}_n\left[P_{\mathrm{o}}(n)\right]$ means the average outage probability across all RIS tiles, thus $\mathbb{E}_n\left[P_{\mathrm{o}}(n)\right] - P_{\mathrm{o}}(n)$ accounts for the outage probability gap between tile n and across all RIS tiles in $\mathcal{N}$. The selected tiles with $\rho_n = 1$ should have lower outage probability than $\mathbb{E}_n\left[P_{\mathrm{o}}(n)\right]$ so that we have a chance to maximize the gap of the average outage between with and without this exclusion policy. However, if the number of selected tiles $\sum_{\mathcal{N}} \rho_n$ is too low, the QoS in terms of achievable channel capacity of the entire RIS system could be reduced; if the number is too high, the utilization efficiency will be diminished as abundant tiles with high outage probability are involved.

In this case, a specific outage threshold G_{th} has been defined for measuring QoS, so the problem (9) will guarantee a reasonable outage probability of the RIS tiles after applying the exclusion strategy while taking into account the utilization efficiency.

To derive a global optimal policy for the exclusion strategy, a threshold is considered on the outage probability $P_{\mathrm{o}}^{\mathrm{th}} \in [\min P_{\mathrm{o}}(n), \max P_{\mathrm{o}}(n)]$, which changes (9) into

$$\max_{P_{\mathrm{o}}^{\mathrm{th}}} \quad \eta\left(P_{\mathrm{o}}^{\mathrm{th}}\right) = \sum_{\mathcal{N}} \mathbf{1}\left(P_{\mathrm{o}}^{\mathrm{th}} > P_{\mathrm{o}}(n)\right)\left(\mathbb{E}_n\left[P_{\mathrm{o}}(n)\right] - P_{\mathrm{o}}(n)\right), \tag{10}$$

$$\text{s.t.} \qquad P_{\mathrm{o}}^{\mathrm{th}} \in [\min P_{\mathrm{o}}(n), \max P_{\mathrm{o}}(n)]. \tag{11}$$

Next, we find the optimal solution to the objective function in (10).

Let n_{th} index the RIS tile whose outage probability is closest to $P_{\mathrm{o}}^{\mathrm{th}}$ as

$$n_{\mathrm{th}} = \arg\min_{n\in\mathcal{N}} \|P_{\mathrm{o}}^{\mathrm{th}} - P_{\mathrm{o}}(n)\|. \tag{12}$$

Hence, the number of the tiles with $P_{\mathrm{o}}(n)$ less than $\mathbb{E}_n\left[P_{\mathrm{o}}(n)\right]$ equals to n_{th}, in another word, $\sum_{\mathcal{N}} \mathbf{1}\left(P_{\mathrm{o}}^{\mathrm{th}} > P_{\mathrm{o}}(n)\right) = n_{\mathrm{th}}$. Given the monotonic increase of $P_{\mathrm{o}}(n)$ with respect to n, the following holds true

$$\frac{\partial}{\partial P_{\mathrm{o}}^{\mathrm{th}}}\eta = \frac{\partial}{\partial P_{\mathrm{o}}^{\mathrm{th}}}\left(n_{\mathrm{th}}\mathbb{E}_n\left[P_{\mathrm{o}}(n)\right] - \sum_{n=1}^{n_{\mathrm{th}}} P_{\mathrm{o}}(n)\right), \tag{13}$$

To continue this derivation, one should notice that due to (12), n_{th} is the index of $P_{\mathrm{o}}^{\mathrm{th}}$ among the feasible outage probability value domain. Thus any slight change to $P_{\mathrm{o}}^{\mathrm{th}}$ leads to a directly proportional change in n_{th} as $\Delta n_{\mathrm{th}} \propto \Delta P_{\mathrm{o}}^{\mathrm{th}}$. Then, we have

$$\begin{aligned}(13) \implies \frac{\partial}{\partial P_{\mathrm{o}}^{\mathrm{th}}}\eta &\propto n_{\mathrm{th}}\mathbb{E}_n\left[P_{\mathrm{o}}(n)\right] - \sum_{n=1}^{n_{\mathrm{th}}} P_{\mathrm{o}}(n) - \left[\left(n_{\mathrm{th}}-1\right)\mathbb{E}_n\left[P_{\mathrm{o}}(n)\right] - \sum_{n=1}^{n_{\mathrm{th}}-1} P_{\mathrm{o}}(n)\right] \\ &= \mathbb{E}_n\left[P_{\mathrm{o}}(n)\right] - P_{\mathrm{o}}^{\mathrm{th}}.\end{aligned} \tag{14}$$

We also note that

$$\frac{\partial^2}{\partial (P_{\mathrm{o}}^{\mathrm{th}})^2}\eta = \frac{\partial}{\partial P_{\mathrm{o}}^{\mathrm{th}}}\left(\mathbb{E}_n\left[P_{\mathrm{o}}(n)\right] - P_{\mathrm{o}}^{\mathrm{th}}\right) = -1 < 0, \tag{15}$$

which indicates the objective function (10) is concave.

To get the optimal policy, we need to solve $\frac{\partial}{\partial P_{\mathrm{o}}^{\mathrm{th}}}\eta = 0$, which leads to an exclusive solution

$$P_{\mathrm{o}}^{\mathrm{th}} = \mathbb{E}_n\left[P_{\mathrm{o}}(n)\right]. \tag{16}$$

Please note that (16) yields the only solution to the optimization problem (9) or (10). Hence, the following mapping holds true

$$\rho_n = \mathbf{1}\left(\mathbb{E}_n\left[P_{\mathrm{o}}(n)\right] > P_{\mathrm{o}}(n)\right), \tag{17}$$

which implies that the optimal strategy in this case is to exclude the RIS tiles whose outage probabilities are higher than the average outage probability among all tiles. This optimal solution requires a search with complexity of $\mathcal{O}(N)$ where N is the total number of RIS tiles across the room. This low complexity is due to the fact that the optimal solution requires to find the average value among the tiles based on the statistics of outage probabilities.

Remark: Please note that one might consider a very straightforward formulation focusing on minimizing the outage probability rate among the selected RIS tiles. However, such a formulation just yields to an extreme solution that is to minimize the selected number of RIS tiles. This type of wrong definition could be or at least contain the following component,

$$\min_{\rho_n \in \{0,1\}} \eta(\rho_n) = \frac{\sum_{\mathcal{N}} \rho_n P_{\mathrm{o}}(n)}{\sum_{\mathcal{N}} \rho_n}.$$

This objective metric η monotonically increases as we keep increasing the number of selected RIS tiles, hence, the optimal ρ_n is to activate the only one tile with the lowest outage probability. This solution damages the resultant channel gain and capacity since minimizing the RIS tile number also means the reduction of the RIS coverage, capacity, and possible functions. Therefore, the constraint of this problem curled into the efficiency dimension, where we need to balance the reduction of RIS control overhead and the cost of RIS performance due to the reduction of RIS tile number.

B. Case 2: Best-Effort Service and Efficient Utilization of RIS

In this case, the focus is on maximizing the RIS channel gains rather than focusing on the outage probabilities. The expectation of the RIS channel gain over the time while considering the channels among all the UEs and APs can be expressed as

$$\Gamma(n) = \mathbb{E}_{t,u,a}\left[G_{\mathrm{o}}(t, n|a, u)\right]. \tag{18}$$

The objective function in this case follows a similar logic as in (9). The order of magnitude of the channel gain $\Gamma(n)$ will be changed according to each wavelength, hence, we need to consider a ratio of channel gain enhancement in the objective formulation. We have

$$\max_{\rho_n \in \{0,1\}} \eta(\rho_n) = \sum_{\mathcal{N}} \rho_n \frac{\Gamma(n) - \mathbb{E}_n\left[\Gamma(n)\right]}{\mathbb{E}_n\left[\Gamma(n)\right]}. \tag{19}$$

where the second term corresponds to the average channel gain among all the tiles without the

adoption of the exclusion strategy and the first term indicates the average channel gain when the exclusion strategy is adopted. Hence, the formulation in (19) aims to balance the enhancement in channel gain due to the RIS tiles and the utilization efficiency of the RIS tiles. Similar to the solution of (9), a global policy is pursued using a threshold on the channel gain expectation, i.e., $\Gamma^{\text{th}} \in \mathfrak{R} \cap [\min \Gamma(n), \max \Gamma(n)]$. Then, (19) can be re-written as

$$\max_{\Gamma^{\text{th}}} \quad \eta\left(\Gamma^{\text{th}}\right) = \sum_{\mathcal{N}} \mathbf{1}\left(\Gamma^{\text{th}} < \Gamma(n)\right) \frac{\Gamma(n) - \mathbb{E}_n\left[\Gamma(n)\right]}{\mathbb{E}_n\left[\Gamma(n)\right]}, \tag{20}$$

$$\text{s.t.} \qquad \Gamma^{\text{th}} \in [\min \Gamma(n), \max \Gamma(n)]. \tag{21}$$

Also, the convexity and the optimal solution to the objective function (20) is obtained as follows. Let the tile index n be ordered such that $\Gamma(n)$ is monotonically decreasing. Therefore, it yields

$$\frac{\partial}{\partial \Gamma^{\text{th}}} \eta = \frac{\partial}{\partial \Gamma^{\text{th}}} \left(\sum_{n=1}^{n_{\text{th}}} \frac{\Gamma(n)}{\mathbb{E}_n\left[\Gamma(n)\right]} - n_{\text{th}} \right), \tag{22}$$

where n_{th} is the RIS tile index of which the channel gain expectation is closest to Γ^{th} as

$$n_{\text{th}} = \arg\min_{n \in \mathcal{N}} \ \|\Gamma^{\text{th}} - \Gamma(n)\|. \tag{23}$$

Since $\Gamma(n)$ is monotonically decreasing with respect to n, we have $\Delta n_{\text{th}} \propto -\Delta \Gamma^{\text{th}}$. Therefore, the following holds true

$$\begin{aligned} (22) \implies \frac{\partial}{\partial \Gamma^{\text{th}}} \eta &\propto \sum_{n=1}^{n_{\text{th}}-1} \left(\frac{\Gamma(n)}{\mathbb{E}_n\left[\Gamma(n)\right]} \right) - (n_{\text{th}} - 1) - \left[\sum_{n=1}^{n_{\text{th}}} \left(\frac{\Gamma(n)}{\mathbb{E}_n\left[\Gamma(n)\right]} \right) - n_{\text{th}} \right] \\ &= -\frac{\Gamma^{\text{th}}}{\mathbb{E}_n\left[\Gamma(n)\right]} + 1. \end{aligned} \tag{24}$$

Then, the objective function (20) is proven to be concave since

$$\frac{\partial^2}{\partial \left(\Gamma^{\text{th}}\right)^2} \eta = \frac{\partial}{\partial \Gamma^{\text{th}}} \left(-\frac{\Gamma^{\text{th}}}{\mathbb{E}_n\left[\Gamma(n)\right]} + 1 \right) = -\frac{1}{\mathbb{E}_n\left[\Gamma(n)\right]} < 0. \tag{25}$$

Meanwhile, (24) has one and only one zero point, which is also the optimal solution to problem (20), i.e.,

$$\Gamma^{\text{th}} = \mathbb{E}_n\left[\Gamma(n)\right]. \tag{26}$$

Consequently, the optimal policy for the decision variable on tile exclusion is given by

$$\rho_n = \mathbf{1}\left(\mathbb{E}_n\left[\Gamma(n)\right] < \Gamma(n)\right), \tag{27}$$

which means that the optimal strategy in this case is to exclude the RIS tiles whose channel gain is less than the average channel gain among all tiles. Again, the complexity of this optimal strategy is $\mathcal{O}(N)$.

C. Complexity of Generating Channel Data Statistics by Conventional Ray-Tracing

The optimal policies described in (17) and (27) require the statistics of the channel data in the PWE. However, it is impractical to consider general distributions for the outage probabilities or channel gain expectation at high frequency bands. Our investigation in [22] has demonstrated that the distribution of the channel gain and outage probability highly depend on the room layout and the spatio-temporal mobility patterns of the users. Consequently, using an accurate indoor mobility model, the indoor wireless channels can be simulated and a heat map can be generated on the walls to capture the channel gain and outage probability at the RIS tiles. The generated heat maps then can be used to find the optimal solutions described in (10) and (20).

Generating the heat maps using Monte-Carlo ray-tracing that assumes random and scattered rays and then judging the ray blockage would incur huge computational complexity that makes this data generation process infeasible. Consider a total of N RIS tiles across the room ($N \sim 6000$ since a wall can accommodate 1500 tiles each with size 10 cm$\times 10$ cm), Y APs, U users, and M objects (e.g., furnishing). We assume that the user body and opaque objects are in the form of cuboids, hence, each contributes 6 surfaces with 24 vertices for blockage judgment. The computational cost for a blockage judgment of a ray is then proportional to $24(U+M)$, since the blockage judgment is based on finding interaction points between a ray and all the surfaces. For the AP-RIS links in the entire room, the computational cost for the ray blockage judgment is proportional to $24NY(U+M)$. Moreover, for the RIS-UE links, this cost is proportional to $24NU(U+M)$, so, for the complete AP-RIS-UE, this is proportional to N^2 ($\sim 10^9$). This complexity is just for one time slot, which accounts for the coherence time of indoor mobility ($\sim$ 100 ms). In practice, the time scale should cover the day to capture various user density scenarios, which would eventually include millions of time slots. Hence, the ray analysis on the surfaces of a room incurs huge computational complexity.

This article has been accepted for publication in IEEE Transactions on Wireless Communications. This is the author's version which has not been fully edited and content may change prior to final publication. Citation information: DOI 10.1109/TWC.2023.3284897

IV. Shadow Area Identification Method

A more efficient approach should be adopted to generate the data needed to solve (10) and (20). Towards this objective, we propose herein a ray-projection-based approach to generate the required heat maps. Blockage judgement is inevitable for any ray-tracing-based channel model whenever diffraction-limited bands and opaque objects are involved. In the conventional ray-tracing, one have to decide for each ray of the 10^9 rays if it is blocked or not by checking the interaction of each ray with each user/object in the room. Considering the complexity of conventional blockage judgement mentioned in Section III-C, the objective in this section is to reduce $(24N)^2$ to 1 following an analytical approach. To this end, we propose an analytical and global blockage judgement method that is called once for all the N rays. The core of such a method is based on the concept of look-up-table (LUT) of shadowed rays, which is constructed based on the shadow area identified upon the RIS tiles from the perspective of each ray source point.

A. Proposed Concept of Shadow Area LUT

In the proposed shadow area method, we find the shadow region and any ray in this shadow region is blocked. We establish and update LUT of shadow rays as follows.

Consider an AP located at point $\mathbf{p}_a$, a corner point of a user located at $\mathbf{p}_u$, and a target surface S. One can draw the ray from $\mathbf{p}_a$ to $\mathbf{p}_u$ and obtain a projection point on S as $\mathbf{p}_S$, as shown in Fig. 3(a). The calculation of this projection point $\mathbf{p}_S$ is much faster than checking the interaction between a given ray and each of the five surfaces of a given user or object. For example, consider the projection from (x_a, y_a) to (x_u, y_u) upon the surface with $y = 0$. The projection point is located at $(x_u + y_u(x_a - x_u)(y_u - y_a), 0)$, as shown in Fig. 3(a). Now, consider the location points $\mathbf{P}_{\mathcal{C}_m}$ for corner set $\mathcal{C}_m$ of object m and $\mathbf{P}_{\mathcal{C}_u}$ for corner set $\mathcal{C}_u$ of user u (four corners of the top surface are shown in Fig. 3(a)). Further, consider a set of APs at location points $\mathbf{P}_{\mathcal{A}}$. Upon surface S, we have the set of projection points from object m as $\mathbf{P}_S \langle \mathbf{P}_{\mathcal{A}} \rightarrow \mathbf{P}_{\mathcal{C}_m} \rangle$, where $\mathbf{P}_S\langle\cdot\rangle$ corresponds to the projection of a group of points. The shadow area under object m's blockage is confined by the boundaries of the set of projection points, which we refer to it by $[\mathbf{P}_S \langle \mathbf{P}_{\mathcal{A}} \rightarrow \mathbf{P}_{\mathcal{C}_m} \rangle]$. Likewise, the shadow area generated by user u can be expressed by the boundaries of $[\mathbf{P}_S \langle \mathbf{P}_{\mathcal{A}} \rightarrow \mathbf{P}_{\mathcal{C}_u} \rangle]$. Therefore, for surface S, the shadow area can be expressed as

$$\mathbf{\Omega}\left(S, \mathbf{P}_{\mathcal{A}}; \mathbf{P}_{\mathcal{C}_m}, \mathbf{P}_{\mathcal{C}_u}\right) = \cup\left(\cup_m \left[\mathbf{P}_S \langle \mathbf{P}_{\mathcal{A}} \rightarrow \mathbf{P}_{\mathcal{C}_m} \rangle\right] \cup_u \left[\mathbf{P}_S \langle \mathbf{P}_{\mathcal{A}} \rightarrow \mathbf{P}_{\mathcal{C}_u} \rangle\right]\right) . \tag{28}$$

This article has been accepted for publication in IEEE Transactions on Wireless Communications. This is the author's version which has not been fully edited and content may change prior to final publication. Citation information: DOI 10.1109/TWC.2023.3284897

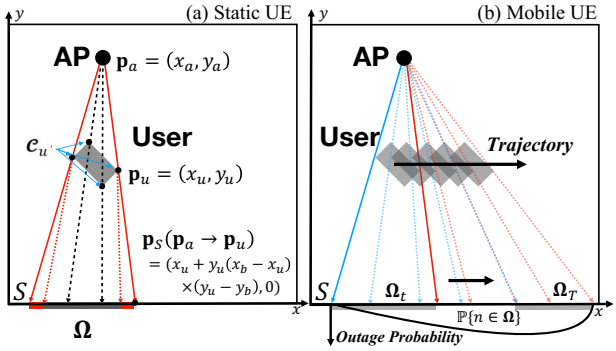

Fig. 3. Illustration of shadow area method for efficient blockage judgments. The basic concept of identifying the shadow area is shown in (a), while (b) demonstrates how UE mobility would affect the shadow area statistic within a period. This is a top-down view. For simplicity, we are showing how objects or users on the ground (distributed in the $x-y$ plane) block rays and cast shadows on the surrounding walls from a top-down perspective.

For a mmWave channel, the channel at the red parts of $\mathbf{\Omega}$, as illustrated in Fig. 3(a), is not necessarily in outage where the channel gain associated with the NLoS components from diffraction and reflection can be calculated based on (3). On the other hand, for VL/IR, the ray directed towards the RIS tiles allocated within the shadow area $\mathbf{\Omega}$ will be blocked, and hence, the channel in the red parts of $\mathbf{\Omega}$, as illustrated in Fig. 3(a), will be in outage.

In the meantime, mobile UEs cause moving shadow areas on the walls as shown in Fig. 3(b). In this illustration, the user is slowing down along the trajectory, which arises the shadow and outage probability along the trajectory direction on the surface. As aforementioned in Section III-C, the time-varying shadow complicates ray-tracing-based methods and is often ignored in literature. Therefore, in this work an efficient shadow region identification method is proposed in Section IV-B.

B. Equivalent Infinite Shadow Projection

The proposed shadow area judgement is a projective transformation problem that can be formally defined as $y = Hx$, given y as the projected the point on the meta-surface (as the vertices in the shadow regions shown in Fig. 4 and Fig. 5) from the source point x with H denoting the linear mapping matrix. In a 3-dementional environment, H is a non-singular 3×3 matrix, which to be estimated needs at least 4 non-collinear points. This estimation of projection matrix needs both the source point and the projective point pairs. However, the projective point is unknown in this problem and thus we cannot rely on the projection matrix-based method.

In this work, we resort to the homography of projective geometry such that we can do segment-to-segment projections for each surface on an object precisely, and eventually to form the holistic

This article has been accepted for publication in IEEE Transactions on Wireless Communications. This is the author's version which has not been fully edited and content may change prior to final publication. Citation information: DOI 10.1109/TWC.2023.3284897

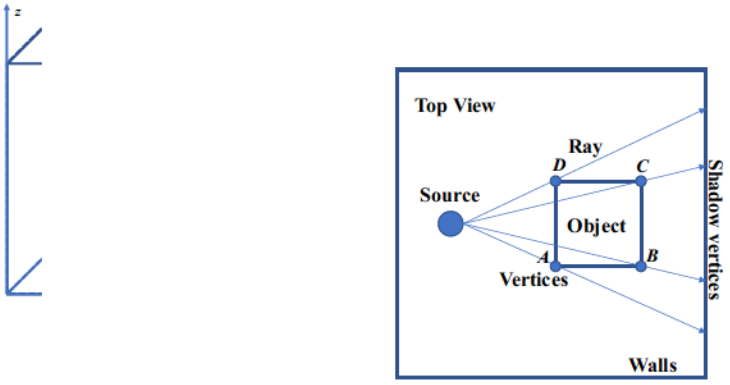

Fig. 4. An illustration of ray tr

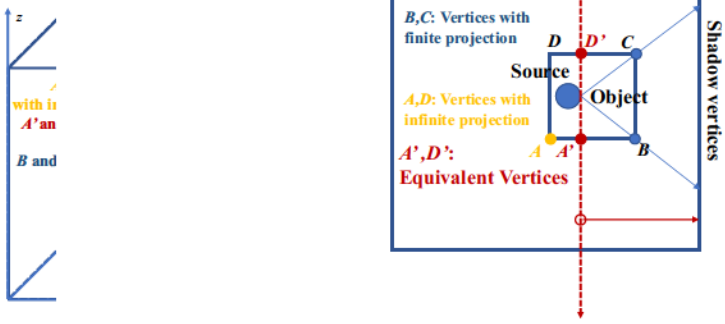

(b) Top view

Fig. 5. An illustration of ray tracing for the shadow shapes by infinite projections.

shape of the shadow upon the RIS tiles induced by a given object. A homography maps one our object surface to the other in the case of pure perspective rotation or a planar scene under one source point. If such a homography exists between the object surface and the projected shadow, four points are sufficient to specify it precisely. As the examples in Fig. 4 and Fig. 5, the vertices on top surface of the object are confined by the 4 edges that are projected into the corresponding edges on the wall to form the shadows.

The challenge in each segment-to-segment projection is the presence of infinite projections as illustrated in Fig. 5. Consider a segment (A, B) in Fig. 5, where A and B corresponds to the two ends of an edge. Suppose we want to find the projection of (A, B) on wall surface W from the view of source S. Let $\|a - b\|_2$ denote the distance from a to b. In Fig. 5, the following relationship holds: $\|A-W\|_2 > \|S-W\|_2 > \|B-W\|_2$, then the end point B can be safely projected on W (finite projection) whereas the projection of A never reaches W (infinite projection) since A is outside the field-of-view (FOV) of $S \rightarrow W$. In this case, the shadow

of this segment is a ray with only one endpoint, which makes the integration of all segment projections to form the whole closed shape impossible.

To address this issue, we propose the *Equivalent Infinite Shadow Projection* (EISP) method to enable the infinite projection of A in Fig. 5 by creating an equivalent substitution vertex point A' that convert the infinite projection into its equivalent finite projection.

The projection calculation must be done in terms of the edge of the object, which means that the projection of both endpoints should be considered simultaneously in order to ensure the homography definition. Given an edge and the associated two endpoints, when an infinite projection point is detected such as $\|A-W\|_2 > \|S-W\|_2$ in Fig. 5, EISP method would be applied to obtain an equivalent endpoint A' first, which can be finitely and safely projected onto the wall. Then using A' to finish the segment (A',B) projection based on a conventional finite projection to get the shadow edge caused by this segment.

This procedure should be done for any two parallel edges of each object surface as these two parallel edges cover all the four vertices. Please note that since we assume all the objects are cuboid, only the top and bottom surfaces are enough to shape the shadow, and the other four side surfaces projections are redundant. To sum up, for each object, four rounds of edge projections are needed. Finally, we integrate all the obtained edge shadows to shape the complete shadow area upon the RIS tiles.

The details of the EISP method for an edge projection are summarized as follows:

- *Assumption*: Let the RIS tiles be located over the walls parallel to X-axis ($y = W_y, \forall x, \forall z$). Denote the subscripts x, y, z for each point as their Cartesian coordinates. Consider an edge with endpoints A and B, where A relates to an infinite projection and B is projected finitely as illustrated in 5. Denote $\mathbf{W}(\cdot)$ as the projection calculation to the target wall surface.

(1) For the two endpoints A and B, check the distance relationship among A, B and W, and get $\|A-W\|_2 > \|S-W\|_2 > \|B-W\|_2$, therefore, A needs infinite projection whereas B can be normally projected on W.

(2) For the finite projection of B, first check if B is located on the surface of W.

  (2.1) If so, the projection coordinate of B equals to B itself as $\mathbf{W}(B) = B$, which means point B coincides with its shadow.

  (2.2) If not, according to the geometric relations among the source point, the vertex and

This article has been accepted for publication in IEEE Transactions on Wireless Communications. This is the author's version which has not been fully edited and content may change prior to final publication. Citation information: DOI 10.1109/TWC.2023.3284897

the shadow point to be calculated, the projection shadow coordinate of B equals to

$$\mathbf{W}(B) = \begin{pmatrix} \left(S_x - B_x \frac{S_y - W_y}{B_y - W_y}\right) \Big/ \left(1 - \frac{S_y - W_y}{B_y - W_y}\right) \\ W_y \\ \left(S_z - B_z \frac{S_y - W_y}{B_y - W_y}\right) \Big/ \left(1 - \frac{S_y - W_y}{B_y - W_y}\right) \end{pmatrix}.$$

(3) For the infinite projection of A, first find the equivalent endpoint A' to replace A, according to the geometric relations among the edge (A, B) and the source S shown in Fig. 5(b), the coordinate of A' is obtained as

$$A' = \begin{pmatrix} (B_x - A_x)(A_y - S_y)/(A_y - B_y) + A_x \\ S_y + \delta \cdot \mathrm{sgn}(W_y - S_y) \\ B_z \end{pmatrix},$$

where δ denotes a small positive interval to avoid "division by zero" in the next step.

(4) Then, the newly updated equivalent endpoints A' is used to carry out the substitute finite projection, it yields the shadow coordinate as

$$\mathbf{W}(A) = \mathbf{W}(A') = \begin{pmatrix} \left(S_x - A_x \frac{S_y - W_y}{A_y - W_y}\right) \Big/ \left(1 - \frac{S_y - W_y}{A_y - W_y}\right) \\ W_y \\ \left(S_z - A_z \frac{S_y - W_y}{A_y - W_y}\right) \Big/ \left(1 - \frac{S_y - W_y}{A_y - W_y}\right) \end{pmatrix}.$$

(5) Finally, $(\mathbf{W}(A), \mathbf{W}(B))$ is yielded as the projected shadow of the edge (A, B) upon the wall W.

This is an example for the projection on the wall parallel to X-axis ($y = W_y, \forall x, \forall z$); yet, when projecting toward the walls parallel to Y-axis ($x = W_x, \forall y, \forall z$), just exchange the coordinations of x and y.

C. Complexity

The computational cost for the calculation of $\mathbf{\Omega}$ is proportional to $4Y(U+M)$ and $4U(U+M)$ for the AP-RIS and RIS-UE links, respectively. Hence, the reduction in the overall computational complexity can be expressed as $6\Delta N$, where Δ denotes the computation time ratio of ray-surface-intersection judgment and ray-projection point calculation. The judgment of ray-surface-

intersection involves the point in polygon problem [31], which is a time-expensive search problem [32]. However, the projection point is calculated analytically, which is much faster than solving a search problem. Hence, Δ is also a considerable large number. To sum up, the computational complexity is notably reduced, such that the data generation and analysis for complete mobile trajectories are possible.

V. Results and Discussions

In this section, we investigate all the layouts described in Section II while being covered in the white-light band (referred to as 'Li'), the 28 GHz mmWave band (referred to as '28GHz'), or the 73 GHz mmWave band (referred to as '73GHz'). First, the implementation details of the proposed optimal exclusion strategy of ineffective RIS tiles are summarized. Second, numerical results are presented and discussed. In what follows, the QoS guarantee case is referred to as 'QoS' and the best effort service case is referred to as 'BES'.

A. Implementation Details

The implementation of the proposed optimizations requires two major procedures, namely, RIS channel dataset preparation and optimal RIS tile exclusion based on the channel statistics. The steps of each procedure are detailed below.

1. RIS Channel Dataset Preparation:

(1.1) *Terminal Mobility Generation:* User mobility details are generated with 6-D trajectories including 3-D space position traces and 3-D terminal orientation records. This follows the procedure summarized in Section II-B and detailed in [22].

(1.2) *Identification of Shadow Areas:* Given the multi-user trajectory dataset and the corresponding indoor layouts, the EISP method detailed in Section IV-B is used for each trace to identify the spatial shadow distributions. Based on the specification of the shadow regions, LUT of shadowed rays is established.

(1.3) *RIS Tile LoS Data Generation:* Given the shadow distribution map, the RIS tiles outside the shadow areas are identified and their LoS channel gains are calculated following a conventional ray-tracing method and the proper channel model in Section II-C and II-D.

(1.4) *RIS Tile NLoS Data Generation:* For the tiles inside shadow, the LoS channel components are lost, yet, the mmWave NLoS component from reflections and diffractions can be distinguishable over the background noise of receivers according to Section II-C.

2. Optimal RIS Tile Exclusion Using the RIS Channel Statistics:

(2.1) *Optimal Exclusion Conditions Using the RIS Channel Statistics:* Using the RIS channel data statistics, the expectations of channel gains and outage probabilities from the perspective of each RIS tile are calculated. The expectations are calculated over UEs, APs, time, and tiles for each wall.

(2.2) *Optimal Tile Exclusion Deployment:* The aforementioned expectations are used as the thresholds for making decisions on the exclusion areas of RIS tiles following the rules in (17) and (27) for each case, respectively.

B. Effectiveness of the Optimizations of the Exclusion Thresholds

This subsection justifies the proposed optimal strategy on the exclusion area selection based on the comparison with an exhaustive search method. Fig. 6 illustrates these comparisons, where the curves track the objective functions η_{QoS} and η_{BES} during the exhaustive searches, whereas $\eta_{\text{QoS-opt}}$ and $\eta_{\text{BES-opt}}$ denote the optimal results indicated by the proposed statistical-based solutions.

Remark: Please note that we obtain both metrics of η_{QoS} and η_{BES} for the two cases at the same time as will be discussed bellow. Although η_{QoS} and η_{BES} seem to be two different indicators, both of them are the measures of performance of the exclusion strategies in essence. η_{QoS} and η_{BES} are not unique to any single strategy, as they can be obtained regardless of the strategy used.

Fig. 6(a) investigates the QoS guarantee case. Using a conventional exhaustive search method, we first sweep the parameter of P_{o}^{th} among its feasible domain. Then, we execute the rule in (17). The main objective here is to validate the optimal solution in (16) and also study whether the QoS guarantee case covers the best effort service case. During the sweep of P_{o}^{th}, the optimal solution in $\eta_{\text{QoS}}(P_{\text{o}}^{\text{th}})$ is demonstrated for the single user case and the most crowded density as well. These curves also illustrate the trade-off between the outage rate reduction and the exclusion rate. For instance, in Fig. 6(a), the metric η_{QoS} reflects the outage rate reduction performance, while the thresholds indicates the exclusion rate. An exclusion rate that is too high or too low does not result in optimal outage rate reduction performance, and the optimal exclusion rate needs to be chosen as a compromise according to (17). This fact unveils an attribute hidden inside the

This article has been accepted for publication in IEEE Transactions on Wireless Communications. This is the author's version which has not been fully edited and content may change prior to final publication. Citation information: DOI 10.1109/TWC.2023.3284897

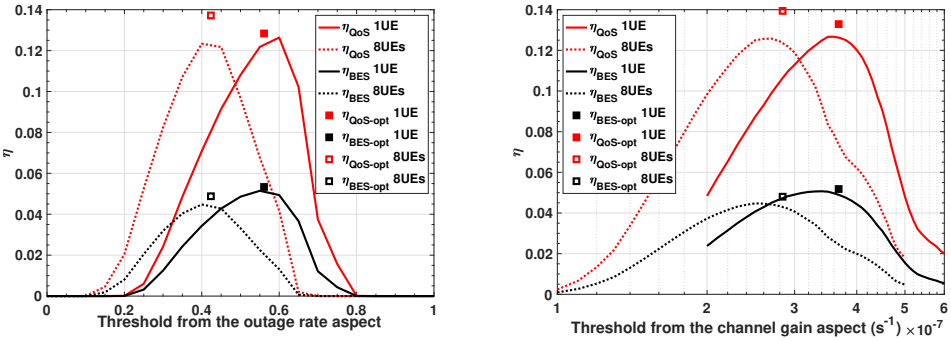

(a) Case 1: QoS-method (b) Case 2: BES-method

Fig. 6. Effectiveness of optimizations depicted by the result comparison of our proposed optimization and the exhaustive search method. The demonstrated results are obtained in the R1 layout with 9 APs operating in 28 GHz mmWave through 1 to 8 UEs. The analysis and discussion for the presented setup can be generalized to the others, but have been omitted due to space limitation.

outage distribution map such as in Fig. 7(a) and (c), where the outage distribution (illustrated by its complementary metric as survival ratio) seems convex with one single minimal location on the wall. Therefore, the sweep starting from a low $P_{\mathrm{o}}^{\mathrm{th}}$ means including the tiles around the minimal outage rate locations first, and these tiles will not contribute to a high reduction amount in $\eta_{\mathrm{QoS}}(P_{\mathrm{o}}^{\mathrm{th}})$ due to their small area in total. Thus, the metric in (10) drives the optimizer to limit the exclusion area by lifting $P_{\mathrm{o}}^{\mathrm{th}}$, which gradually increases $\eta_{\mathrm{QoS}}(P_{\mathrm{o}}^{\mathrm{th}})$. However, as $P_{\mathrm{o}}^{\mathrm{th}}$ continues to rise up until higher than $\mathbb{E}_n\left[P_{\mathrm{o}}(n)\right]$, such a contraction on the exclusion area comes with a cost in η_{QoS} since the newly involved tiles whose $P_{\mathrm{o}}(n)$ is very high negatively affects the cumulative value of $\eta_{\mathrm{QoS}}(P_{\mathrm{o}}^{\mathrm{th}})$. This phenomenon experimentally verifies that objective function (10) is convex.

After choosing $\rho_n = \mathbf{1}\left(\mathbb{E}_n\left[P_{\mathrm{o}}(n)\right] > P_{\mathrm{o}}(n)\right)$, we get the optimal results in Fig. 6(a). With this strategy, we can simultaneously evaluate the both metrics of η_{QoS} and η_{BES}. Obviously, the optimal $P_{\mathrm{o}}^{\mathrm{th}}$ yields the peak values of η_{QoS} and η_{BES} regardless of the user density. More importantly, this optimal $P_{\mathrm{o}}^{\mathrm{th}}$ is easy to obtain with an overall complexity of $O(4(U+M)(U+Y)+N)$, in which the complexity for data generation is $O(4(U+M)(U+Y))$ and its expectation is estimated with only a complexity of $O(N)$.

In Fig. 6(b), the best effort service case is examined. The logic of argument here is similar to the previous case, starting with a conventional exhaustive search method to sweep the parameter of Γ^{th} within its feasible domain. The curves of $\eta_{\mathrm{BES}}\left(\Gamma^{\mathrm{th}}\right)$ prove the convexity of the objective function in (20) regardless of the user density.

Meanwhile, this convexity is induced by the trade-off between the cumulative channel gain

enhancement from the RIS tiles and the exclusion rate. In Fig. 6(b), the metric η_{BES} reflects the cumulative channel gain enhancement, and the thresholds implies the exclusion rate. The optimal exclusion rate lays in the sole and maximum point in Fig. 6(b) as theoretically proved in (27). A higher or lower exclusion rate will jeopardize the channel gain enhancement.

We find the proposed optimal strategy yields a slightly higher η performance than the highest value of the exhaustive search, which indicates the benefits from applying our proposed strategy. Such a difference can be attributed to the smaller step size of 0.1 used in the exhaustive search, which is not sufficient for achieving the higher resolution required by the optimal solution. Achieving such an optimal solution with an exhaustive search means raising complexity tremendously. Moreover, conducting an exhaustive search with a high complexity that requires testing every possible decision to exclude the shadowed RIS tiles is impractical for real-world scenarios, where the channel data may last for several hours or even longer. Therefore, the choice of step size for the exhaustive search is a trade-off between accuracy and practicality given the underlying complexity. Nonetheless, our proposed method demonstrates its superiority in complexity and accuracy, providing the optimal result with only one test case.

Follow this logic, we refer to the channel gain distribution demonstrated by Fig. 7(b) and (d). The channel gain distribution approximates to convexity with one maximal area nearby the center. Therefore, when Γ^{th} is low, the exclusion area is so reduced such that the value of (20) approaches to zero since $\sum_{\mathcal{N}} \Gamma(n) \approx \sum_{\mathcal{N}} \mathbb{E}_n [\Gamma(n)]$ when the exclusion number is close to the number of zero. Then, as Γ^{th} increases, the value of (20) increases until $\Gamma^{\text{th}} = \mathbb{E}_n [\Gamma(n)]$ since the number of included tiles decreases and there are still tiles in this area whose channel gain is lower than $\mathbb{E}_n [\Gamma(n)]$. Once $\Gamma^{\text{th}} > \mathbb{E}_n [\Gamma(n)]$, in such an exclusion area, the tiles with higher channel gain beats over the lower ones, thus, the metric of cumulative channel gain enhancement is decreased. This fact proves our theory on the convexity of the objective of (20).

The implementation of $\rho_n = \mathbf{1} (\mathbb{E}_n [\Gamma(n)] < \Gamma(n))$ generates the optimal solutions as shown in Fig. 6(b). In this case, we also evaluate the both metrics of η_{QoS} and η_{BES}. Again, the results verifies that the proposed solution covers both the cases regardless of the user density since $\eta_{\text{QoS-opt}}$ and $\eta_{\text{BES-opt}}$ for 1 UE to 8 UEs locate at the same threshold decision. The overall solution complexity is still $O(4(U+M)(U+Y)+N)$.

To conclude this subsection, we would like to emphasize that the fundamental component that enables the proposed strategies is the proposed shadow area method. A conventional ray-tracing-based data generation approach and an exhaustive search optimization method would

This article has been accepted for publication in IEEE Transactions on Wireless Communications. This is the author's version which has not been fully edited and content may change prior to final publication. Citation information: DOI 10.1109/TWC.2023.3284897

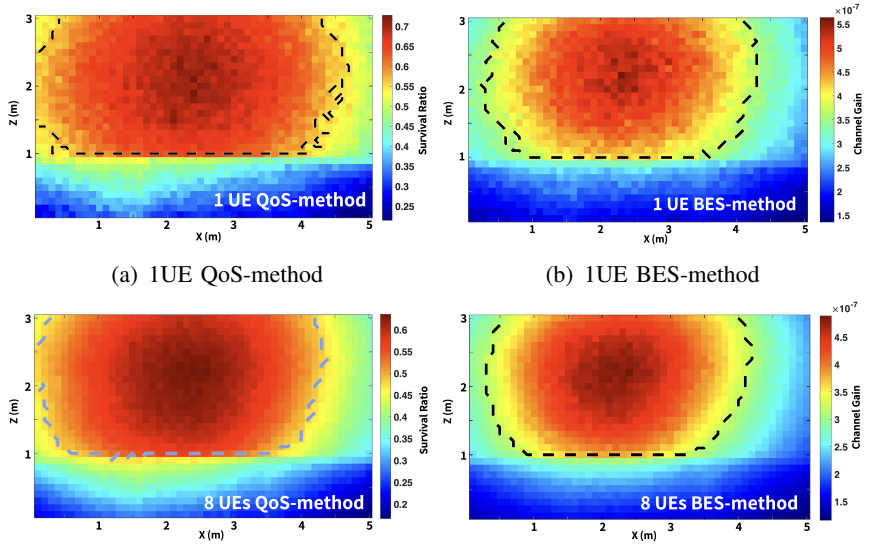

(a) 1UE QoS-method (b) 1UE BES-method

(c) 8UEs QoS-method (d) 8UEs BES-method

Fig. 7. The impact of UE density on the exclusion strategy, survival ratio distribution in (a) and (c), and equivalent channel gain distribution in (b) and (d) illustrated by the heat maps. The excluded regions are those outside the dash-lines. The survival ratio is defined as $1 - P_{\mathrm{O}}$. The demonstrated results are obtained in the R1 layout with 9 APs operating in 28 GHz mmWave supporting 1 and 8 UEs. The analysis and discussion for the presented setup can be generalized to the others, but have been omitted due to space limitation.

not practically solve this problem due to the associated time complexity. On the other hand, the shadow area method makes the data generation process very effective, which makes the statistical analysis and the relevant optimization procedures possible.

C. Impact of User Density

Another concern related to the proposed strategies is their generalization ability and robustness once encountering changes in user density. Due to the time-varying nature of channel statistics under crowd mobility, the user density varies over time. Therefore, we aim to answer the following questions: (a) Do we have to refine the proposed strategies to adapt to various user densities? (b) Under which user density can we condense one single strategy that covers other densities? This subsection is going to answer these questions with numerical evidences based on the optimal solutions.

In the layouts listed in Section II, there are two extreme user densities, i.e., 1 UE and 8 UEs and between them, the user density varies following the proposed mobility model. Thus, it is interesting and representative to investigate how the corresponding strategies differ based on the user density. The results in Fig. 7 show the relationship between the exclusion area in the two extreme user densities. We first show the survival ratio and channel gain maps on the

RIS-equipped wall located at the right-hand side of the door. In the illustration of Fig. 7(a) and Fig. 7(c), the survival ratio is defined as $1 - P_{\mathrm{O}}$. The survival ratio under 8 UEs is less than the 1 UE case by more than 10%on almost every tile. The shadow caused by the meeting desk is clearly demonstrated at the lower region, where the survival ratio is less than 40% in the 1 UE case and 30% in the 8 UEs case. The peak survival ratio region is located at the left-top section of this wall since the UEs usually point at the higher half of the wall and most of the mobility is concentrated near the entrance (at the left side of this wall). Similar patterns can be found in Fig. 7(b) and Fig. 7(d) in terms of channel gain statistics. The channel gain of 1 UE is higher than the 8 UE case by over 20% for each tile. The shadow by the desk is also outlined obviously.

As for the exclusion decision, the region outside the dash-line should be excluded according to the QoS-based strategy in Fig. 7(a) and Fig. 7(c) as well as the BES-based strategy in Fig. 7(b) and Fig. 7(d). The dash lines in fact step over the RIS tiles with the mean value of outage rate or channel gain, where the channel performance of tiles outside the circle is worse than the average and those tiles should be excluded to reduce signaling overhead. Fig. 7 (b) and (d) depict respectively the BES-based strategies for 1 UE and 8 UEs, where the exclusion area for 8 UEs is slightly larger than 1 UE and the inclusion area (inside the dashed-line) of 8 UEs is a subset of that for the 1 UE case. The overlap occupies about 97.11% of the inclusion area for the lowest user density. This fact holds true for the QoS-based method as illustrated in Fig. 7 (a) and (c). However, the overlap increases to nearly 99% of the lowest user density. Although these figures are obtained in one layout, the analysis and discussion can be generalized to other bands and layouts, which however, have been omitted due to space limitation.

The small difference in overlap reflects in the overall performance as characterized in the domain of η as shown in Fig. 6. We find that the user density shifts the peak locations in the two cases, where higher density requires lower outage rate thresholds and lower channel gain thresholds. If one chooses a strategy from 1 UE setup when encountering 8 UEs, one will get more loss in η_{QoS} than in η_{BES}, and vice versa. This implies that the proposed BES-based method offers a better generalization ability against crowd mobility.

To sum up, the proposed exclusion strategies are proven valid for all possible user densities. Also, it is confirmed that the highest density setup yields the most compact, strict, and conservative strategy, and the lowest one leads to a loose strategy. This means that we can deploy the proposed strategies while considering the most crowded setup to cover all the variation in

This article has been accepted for publication in IEEE Transactions on Wireless Communications. This is the author's version which has not been fully edited and content may change prior to final publication. Citation information: DOI 10.1109/TWC.2023.3284897

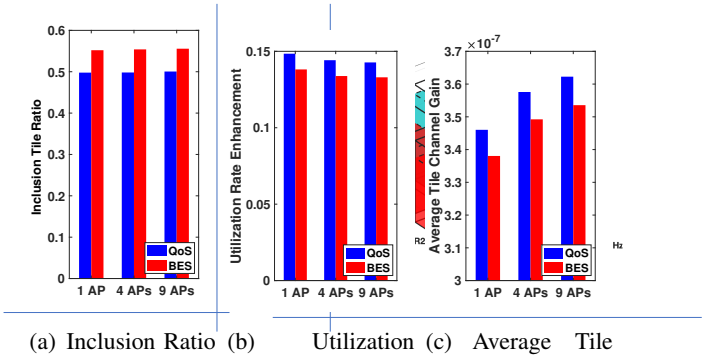

(a) Inclusion Ratio (b) Utilization Rate Increase (c) Average Tile Channel Gain

Fig. 8. The impact of AP number from the perspectives of (a) inclusion ratios, (b) utilization enhancement, and (c) tile channel gain average. The demonstrated results are obtained in the R1 layout with 1 to 9 APs operating in 28 GHz mmWave supporting 8 UEs. The analysis and discussion for the presented setup can be generalized to the others, but have been omitted due to space limitation.

user density over time since it gives the most strict result. Meanwhile, if we care more about the implementation complexity in multiple user data generation but rather than the solution accuracy on area division, we can just run this proposed BES-orientated algorithm under the single UE setup as the solution overlap and generalization is considerable. The single UE data generation costs the lowest complexity but would in turn slightly decrease the BES-based decision accuracy when encountering more crowd cases. Please note that this judgment holds solely for this perspective, and these generalization benefits from the BES-based strategy do have some costs as will be interpreted next.

D. Impacts of Access Point Density

In practice, the AP density would not change over time within a confined layout. However, to explore the impact of RIS-AP interactions on the proposed strategies, we vary the number and location of APs in the room layouts. Our investigation regarding the impact of AP density focuses on three aspects (a) RIS tile exclusion rate defined by the proportion of the excluded tiles among all the tiles, (b) RIS utilization rate, which indicates the outage rate reduction after adopting the proposed optimal strategies, and (c) average channel gain of the included RIS tiles.

Fig. 8(a) shows the RIS tile exclusion rate under the optimal strategies. Firstly, the proposed strategies can merely use around 50% to 55% of RIS tiles to support the communications in the room, which implies a huge reduction in signalling overhead by same percentage. Secondly, we find that the number of APs barely influences the exclusion rate. This means that the proposed strategies performs stably when facing new AP deployments. Moreover, the BES-based strategy clearly requires more tiles at about 5%. This fact is due to the nature of the

best-effort service since it promotes a smaller exclusion area than QoS-based method, as shown in Fig. 7. Furthermore, this also explains why we claimed that the benefits of the BES-based strategy come with a cost, as demonstrated in Fig. 8(b) and (c).

Fig. 8(b) gives the utilization rate enhancements when the proposed strategies are adopted. Such enhancements are derived from the outage proportion reductions due to the optimal selection on the RIS tiles. These enhancements slightly decrease as the AP number increases. This is because the AP coverage has already been improved along with the AP density increase, and consequently the margin for the utilization rate enhancements decrease. Also, the QoS-orientated strategy overpowers the BES-based one since, as we interpreted earlier, the BES-based strategy involves larger outage area with a lower tolerance on outage probability.

Fig. 8(c) presents the average channel gain of the inclusion tiles. First, the increase of AP number brings a higher channel gain average. When it comes the comparison between the QoS and BES-based methods, the latter is more adventurous, which however, reduces the average channel gain. This is counter-intuitive considering the objective of the BES-based method should be maximizing the RIS channel gain. The reason behind this fact is that the problem definition in (20) focuses on the global summarization on the channel gain increase due to the exclusions, but not the average level for each tile. We note that some of the inclusion area in the difference of the two methods are with high channel gain dynamics, thus, the summarization on the channel gain increase is indeed satisfactory based on the BES-based metrics, but some of the overmuch outages are also included. However, when considering more on the outage rate by the QoS-based strategy, the inclusion tiles are less likely to be outage, which in turn rises up the channel gain average.

To sum up here, we prove again the effectiveness of the proposed strategies, and also conclude a satisfactory adaption against the AP densities.

E. Impacts of Environment and Propagation Feature

The sensitivity of high-frequency bands to environment and mobility motivates the adoption of RIS tiles. In this work, we comprehensively investigate the performance of the proposed strategies in diverse environment layouts and equipping with various bands from 28 GHz to the light frequency. We involve the same three key evaluation metrics in Section V-D. Fig. 9(a) and (b) confirm our previous findings on the comparison of QoS and BES-based strategies in Section

This article has been accepted for publication in IEEE Transactions on Wireless Communications. This is the author's version which has not been fully edited and content may change prior to final publication. Citation information: DOI 10.1109/TWC.2023.3284897

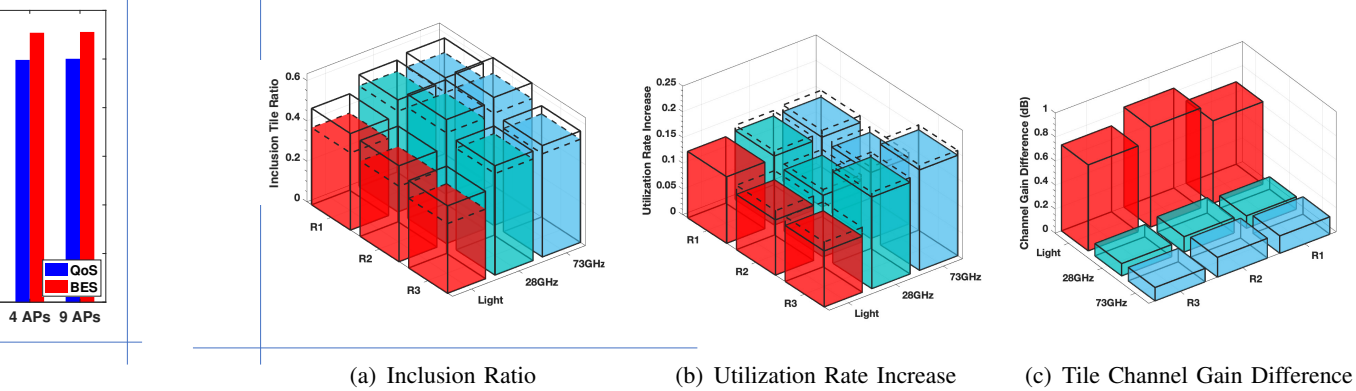

(a) Inclusion Ratio (b) Utilization Rate Increase (c) Tile Channel Gain Difference

Fig. 9. The impact of layouts and wavelengths from the perspectives of (a) inclusion ratios, (b) utilization enhancement, and (c) tile channel gain difference. The demonstrated results are obtained in R1 to R3 layouts with 4 APs operating in white-light, 28 GHz and 73 GHz mmWave supporting 8 UEs.

V-D but with more dimensions. We in this subsection focus on the impacts of the layout change and wavelengths.

Through Fig. 9(a) we find the layout with nine desks inside (R2) gets the highest inclusion rates in all bands. This is mainly because the aisles among the desks yield the extra LoS paths, whereas in the other two layouts, the low areas are shadowed by the desks. This fact is reflected the most in the layout R3 since the desks are against the wall, which give it more margin in the utilization rate increase as shown in Fig. 9(b). For the same reason, in the layout of R2, we get the lowest utilization rate increase. Fig. 9(a) gives the increases in channel gain average after optimizing the exclusions. Since we have more LoS links to leverage by involving the tiles, R2 gets the highest channel gain improvement.

The light band, as shown in Fig. 9(a), is with the highest exclusion rate as about 40% due to the highest outage probability and the lack of diffractions. The average inclusion rates for the two mmWave bands are about 50% to 60%. Interestingly, the 73 GHz band, whose diffraction ability and path loss are worse than 28 GHz, gets slightly less exclusions. The 73 GHz band also gets the highest utilization enhancement, yet the light band gets the lowest. We speculate that the reason is the coverage ability of 28 GHz is already sufficient; and the light band is over the peak performance an RIS system could reach, at least in terms of the RIS system efficiency. Yet there is still good news for the RIS-assisted light band, as shown in Fig. 9(c), as the light band obviously gains the highest channel gain enhancement.

To sum up, the proposed strategies are proven effective and efficient regardless of the environment or the wavelength. The performance gain from the RIS system differs due to the

gaps in the mobility details subject to the environment and the propagation ability especially the diffractions.

VI. Conclusions

This paper aspires to fill the gap in existing research by grasping and tackling the implications of crowd mobility in order to enable practical and efficient engagement and exclusion of indoor PWEs. We defined convex optimization problems in the case of both guaranteed RIS QoS and efficient utilization and best-effort service and efficient utilization of RIS. The optimization takes into account the trade-off among RIS performance, utilization efficiency and RIS control overheads. The solution to this problem is analytically reachable and solely determined by the statistics of the RIS channel. To achieve such an RIS channel statistic, we propose an indoor RIS channel generation method empowered by the practical human mobility patterns and equipped with various wireless mediums. However, a conventional ray-tracing-based channel data generator is paralyzed by the complexity in the ray-blockage judgment. To this end, we propose shadow area identification method and a numerical simplification of the Equivalent Infinite Projection. This methodology enables ray-tracing ray-blockage judgement in a manner of look-up tables. With all these proposed methodologies, we validated our ideas in three typical indoor scenarios and three promising wireless bands. The numerical results justify that the signaling overhead can be reduced by 45%-50%, the tile utilization can be increased by nearly 15%. The case study also proves that our methodology is compatible under the variations of mobile user density, access point density, indoor layout, and transmission wavelengths. We would like to emphasize that despite the difference in the physical layer of VL/IR and mmWave bands, the provided analytical and decision-making frameworks for them are still consistent.

Appendix

Some of the important notations are summarized in Table I.

TABLE I
Summary of Important Notations

Symbol	Definition	Symbol	Definition	Symbol	Definition	Symbol	Definition
$\mathcal{N}$	RIS tile set	$\mathbf{G}_{\mathrm{m}}^{a-b}$	mmWave channel gain	G_{v}^{a-b}	Optical channel gain	Θ	RIS coefficient matrix
$\mathbf{G}_{\cdot,\mathrm{LoS}}$	LoS channel gain	$\mathbf{G}_{\cdot,\mathrm{NLoS}}$	NLoS channel gain	$L_{\mathrm{LoS\,/\,c,s}}$	Path loss	λ	Wavelength
θ	Elevation angles	γ	Gain factor among sub-rays	$\varrho_{c,s}$	Complex Gaussian path gain	$\mathbf{a}(\cdot)$	RIS array response vector
ϕ	Azimuth angles	d	Transmission distance	X_σ	Shadow fading/factor	ϱ	Random phase
A_{R}	Sensor area	ω	Angle of irradiance	ψ	Receiver incidence angle	Ψ_{c}	Receiver's FOV
T_{S}	Optical transmission response	$\Phi_{1/2}$	Half power angle	k	Number of reflections	N	Number of RIS tiles
Y	Number of APs	U	Number of UEs	M	Number of objects	$P_{\mathrm{o}}(n)$	Outage probability
G_{th}	Outage threshold	ρ_n	Exclusion decision	$\Gamma(n)$	Channel gain expectation	$\eta(\cdot)$	RIS efficiency
$\mathbf{p}_a$	AP location	$\mathbf{p}_u$	UE location	S	Surface with shadow	$\mathbf{p}_S$	Shadow projection point set
m	Object index	n	RIS tile index	u	UE index	a	AP index
$\mathbf{P}_{\mathcal{A}}$	AP location set	$\mathbf{P}_{\mathcal{C}_m}$	Object corner location set	$\mathbf{P}_{\mathcal{C}_\mu}$	UE corner location set	$\mathbf{\Omega}$	Shadow area
(X,Y)	Segment between X and Y	W	Wall surface with RIS	X'	Equivalent endpoint of X	$\mathbf{W}(\cdot)$	Shadow projection

REFERENCES

[1] Z.-Y. Wu, M. Ismail, and J. Wang, "Efficient allocation of intelligent surfaces in programmable wireless environments," in *ICC 2021 - IEEE International Conference on Communications*, 2021.

[2] P. Lin, Q. Song, F. R. Yu, D. Wang, A. Jamalipour, and L. Guo, "Wireless virtual reality in beyond 5g systems with the internet of intelligence," *IEEE Wireless Communications*, vol. 28, no. 2, pp. 70–77, 2021.

[3] E. Basar and H. V. Poor, "Present and future of reconfigurable intelligent surface-empowered communications [perspectives]," *IEEE Signal Processing Magazine*, vol. 38, no. 6, pp. 146–152, 2021.

[4] T. V. Chien, H. Q. Ngo, S. Chatzinotas, and B. Ottersten, "Reconfigurable intelligent surface-assisted massive mimo: Favorable propagation, channel hardening, and rank deficiency," *IEEE Signal Proc. Mag.*, vol. 39, no. 3, pp. 97–104, 2022.

[5] P. Del Hougne, M. Fink, and G. Lerosey, "Optimally diverse communication channels in disordered environments with tuned randomness," *Nature Electronics*, vol. 2, no. 1, pp. 36–41, 2019.

[6] X. G. Zhang, Y. L. Sun, B. Zhu, W. X. Jiang, Q. Yu, H. W. Tian, C.-W. Qiu, Z. Zhang, and T. J. Cui, "A metasurface-based light-to-microwave transmitter for hybrid wireless communications," *Light Sci. Appl*, vol. 11, no. 1, pp. 1–10, 2022.

[7] W. Tang, M. Z. Chen, X. Chen, J. Y. Dai, Y. Han, M. Di Renzo, Y. Zeng, S. Jin, Q. Cheng, and T. J. Cui, "Wireless communications with reconfigurable intelligent surface: Path loss modeling and experimental measurement," *IEEE Trans. on Wirel. Commun.*, vol. 20, no. 1, pp. 421–439, 2021.

[8] S. Abadal *et al.*, "Computing and communications for the software-defined metamaterial paradigm: A context analysis," *IEEE Access*, vol. 5, pp. 6225–6235, 2017.

[9] X. Liu, Y. Liu, Y. Chen, and H. V. Poor, "Ris enhanced massive non-orthogonal multiple access networks: Deployment and passive beamforming design," *IEEE J. SEL. AREA COMM.*, vol. 39, no. 4, pp. 1057–1071, 2021.

[10] S. Ma, W. Shen, X. Gao, and J. An, "Robust channel estimation for ris-aided millimeter-wave system with ris blockage," *IEEE T. VEH. TECHNOL.*, vol. 71, no. 5, pp. 5621–5626, 2022.

[11] A. R. Ndjiongue, T. M. N. Ngatched, O. A. Dobre, and H. Haas, "Toward the use of re-configurable intelligent surfaces in vlc systems: Beam steering," *IEEE Wireless Communications*, vol. 28, no. 3, pp. 156–162, 2021.

[12] Z.-Y. Wu, M. Ismail, E. Serpedin, and J. Wang, "Artificial intelligence for smart resource management in multi-user mobile heterogeneous rf-light networks," *IEEE Wireless Communications*, vol. 28, no. 4, pp. 152–158, 2021.

[13] M. Almekhlafi, M. A. Arfaoui, M. Elhattab, C. Assi, and A. Ghrayeb, "Joint resource allocation and phase shift optimization for ris-aided embb/urllc traffic multiplexing," *IEEE Trans. on Commun.*, vol. 70, no. 2, pp. 1304–1319, 2022.

[14] Z. Wan, Z. Gao, and M.-S. Alouini, "Broadband channel estimation for intelligent reflecting surface aided mmwave massive mimo systems," *IEEE International Conference on Communications (ICC)*, June, 2020.

[15] C. Feng, W. Shen, J. An, and L. Hanzo, "Joint hybrid and passive ris-assisted beamforming for mmwave mimo systems relying on dynamically configured subarrays," *IEEE Internet of Things Journal*, vol. 9, no. 15, pp. 13913–13926, 2022.

[16] M. Najafi, B. Schmauss, and R. Schober, "Intelligent reconfigurable reflecting surfaces for free space optical communications," *ArXiv*, vol. abs/2005.04499, 2020.

[17] C.-X. Wang, Z. Lv, X. Gao, X. You, Y. Hao, and H. Haas, "Pervasive wireless channel modeling theory and applications to 6g gbsms for all frequency bands and all scenarios," *IEEE T. VEH. TECHNOL.*, vol. 71, no. 9, pp. 9159–9173, 2022.

[18] H. Abumarshoud, L. Mohjazi, O. A. Dobre, M. Di Renzo, M. A. Imran, and H. Haas, "Lifi through reconfigurable intelligent surfaces: A new frontier for 6g?," *IEEE Vehicular Technology Magazine*, vol. 17, no. 1, pp. 37–46, 2022.

[19] C. Liaskos, A. Tsioliaridou, S. Nie, A. Pitsillides, S. Ioannidis, and I. F. Akyildiz, "On the network-layer modeling and configuration of programmable wireless environments," *IEEE/ACM Trans. on Net.*, vol. 27, pp. 1696–1713, 2019.

[20] B. Xiong, Z. Zhang, H. Jiang, H. Zhang, J. Zhang, L. Wu, and J. Dang, "A statistical mimo channel model for reconfigurable intelligent surface assisted wireless communications," *IEEE Trans. on Commun.*, vol. 70, no. 2, pp. 1360–1375, 2022.

[21] E. Basar, I. Yildirim, and I. Akyildiz, "Indoor and outdoor physical channel modeling and efficient positioning for reconfigurable intelligent surfaces in mmwave bands," *ArXiv*, vol. abs/2006.02240, 2020.

[22] Z. Y. Wu, M. Ismail, J. Kong, E. Serpedin, and J. Wang, "Channel characterization and realization of mobile optical wireless communications," *IEEE Trans. on Commu.*, vol. 68, no. 10, pp. 6426–6439, 2020.

[23] M. Di Renzo *et al.*, "Smart radio environments empowered by reconfigurable intelligent surfaces: How it works, state of research, and the road ahead," *IEEE J. on Sel. Areas in Commun.*, vol. 38, no. 11, pp. 2450–2525, 2020.

[24] S. Priebe and T. Kurner, "Stochastic modeling of thz indoor radio channels," *IEEE Trans. on Wirel. Commun.*, vol. 12, no. 9, pp. 4445–4455, 2013.

[25] P. Chvojka, S. Zvanovec, P. A. Haigh, and Z. Ghassemlooy, "Channel characteristics of visible light communications within dynamic indoor environment," *J. of Lightw. Tech.*, vol. 33, no. 9, pp. 1719–1725, 2015.

[26] K. Lee, H. Park, and J. R. Barry, "Indoor channel characteristics for visible light communications," *IEEE Commun. Lett.*, vol. 15, no. 2, pp. 217–219, 2011.

[27] D. Brockmann, L. Hufnagel, and T. Geisel, "The scaling laws of human travel," *Nature*, vol. 439, no. 7075, pp. 462–465, 2006.

[28] I. Hemadeh *et al.*, "Millimeter-wave communications: Physical channel models, design considerations, antenna constructions, and link-budget," *IEEE COMMUN SURV TUT*, vol. 20, no. 2, pp. 870–913, 2018.

[29] C. Chen, R. Zhang, W. Wen, M. Liu, P. Du, Y. Yang, and X. Ruan, "Hybrid 3dma for multi-user mimo-vlc," *J. Opt. Commun. Netw.*, vol. 14, pp. 780–791, Oct 2022.

[30] J. M. Kahn *et al.*, "Wireless infrared communications," *Proc. of the IEEE*, vol. 85, no. 2, pp. 265–298, 1997.

[31] Z.-Y. Wu, M. Ismail, E. Serpedin, and J. Wang, "Efficient prediction of link outage in mobile optical wireless communications," *IEEE Transactions on Wireless Communications*, vol. 20, no. 2, pp. 882–896, 2021.

[32] K. Hormann and A. Agathos, "The point in polygon problem for arbitrary polygons," *Comput. Geom. Theory Appl.*, vol. 20, no. 3, pp. 131–144, 2001.